Available online at www.sciencedirect.com
ScienceDirect
Optical Materials 31 (2008) 94–101
OPTICAL Materials
www.elsevier.com/locate/optmat

Spectroscopic characterization of Ho^{3+} doped $PbWO_4$ crystals for laser and stimulated Raman scattering applications in the mid-infrared spectral range

Ilya S. Mirov [a,b,1], Vladimir V. Fedorov [a,*], Igor S. Moskalev [a], Dmitri V. Martyshkin [a], Sergey Yu. Beloglovski [c], Stanislav F. Burachas [c], Yuri A. Saveliev [c], Alexander M. Tseitline [c]

[a] *Center for Optical Sensors and Spectroscopies, Department of Physics, University of Alabama at Birmingham, 310 Campbell Hall, 1300 University Boulevard, Birmingham, AL 35294, USA*
[b] *Vestavia Hills High School, 2235 Lime Rock Road, Vestavia Hills, AL 35216, USA*
[c] *North Crystals America, 48 Weston Street, Suite 5, Waltham, MA 02453, USA*

Received 11 November 2007; received in revised form 21 January 2008; accepted 21 January 2008
Available online 11 March 2008

Abstract

Spectroscopic characterization of Czochralski grown Ho(0.2%–4%):$PbWO_4$ crystals were performed over 0.2–8 μm spectral range. Polarized optical absorption, emission and kinetics of fluorescence of $^5I_8 \Leftrightarrow {}^5I_7$ holmium transitions were studied over 20–300 K temperature interval. The lifetime of $^5I_7$ state in the Ho(0.5%):$PbWO_4$ crystal was measured to be 5.0 ms. The stimulated Raman scattering at 2.5 μm was studied under 1.7 and 2.0 μm excitation.

PACS: 76.30.Kg; 42.55.Rz; 42.55.Ye; 42.70.Hj; 42.65.Dr

Keywords: Ho:$PbWO_4$; Spectroscopy; Luminescence trapping; Stimulated Raman

1. Introduction

In recent years, stimulated Raman scattering (SRS) has become a well-established technique used for shifting the frequency of laser radiation to new spectral regions where direct laser oscillation is not available or ineffective. From this point of view, the solid-state Raman lasers operating in the middle-infrared (mid-IR) spectral range are very attractive for a variety of medical, environmental, and sensing applications.

Lead tungstate $PbWO_4$ (PWO) crystals have been known for several decades for their scintillation properties [1]. Much interest was drawn to these crystals by the fact that they have been selected as a material of choice for scintillation detectors used for the precise electromagnetic calorimeter (EMC) of the CMS experiment suited for the search of the Higgs boson in the intermediate mass region at the Large Hadron Collider (LHC) at CERN [2]. As a result, a rather low-cost growth technique for large scale PWO crystals was developed. Later, interest in PWO crystals further grew because of its interesting properties as a nonlinear solid-state material for the SRS [3–5]. In addition, the crystal structure of tungstate crystals allows the introduction of rare-earth (RE: Nd, Yb, Ho, Er, Tm) impurity ions and the utilization of these doped active

* Corresponding author. Tel.: +1 205 934 5318; fax: +1 205 934 8042.
E-mail addresses: ismirov@gmail.com (I.S. Mirov), vfedorov@phy.uab.edu (V.V. Fedorov), moskalev@uab.edu (I.S. Moskalev), atseitline@northcrystals.com (A.M. Tseitline).
URL: http://www.northcrystals.com (A.M. Tseitline).
[1] Summer 2006 intern at the Center for Optical Sensors and Spectroscopies, Department of Physics, University of Alabama at Birmingham.

0925-3467/$ - see front matter © 2008 Elsevier B.V. All rights reserved.
doi:10.1016/j.optmat.2008.01.010

crystals for lasing accompanied by Raman self-conversion of radiation to a new spectral range. The self oscillation Raman laser based on Nd:PWO crystals was demonstrated in Q-switched mode of operation in [6].

Recently it was demonstrated, that the fiber-bulk (Tm-fiber – Ho-laser) hybrid laser approach of direct laser pumping of the $^5I_7$ manifold of Ho^{3+} ions in YAG and YLF crystals allows effective (up to 85%) conversion of the CW pump at 1.9 μm into a Q-switched 2.1 μm radiation [7–11].

The major objective of this work is to study the spectroscopic characteristics of Ho doped PWO crystals for identification of their feasibility as a combined self-gain Raman medium for the development of an effective fiber-bulk hybrid system operating at room temperature at ~2.5 μm for medical and trace gas analysis applications.

2. Sample preparation

The growth of the experimental Ho:PWO crystals with a diameter of 30 mm and length of 50 mm was done by the Czochralski method in the inert atmosphere from the recrystallized charge obtained from high-purity chemicals using earlier developed technology of mass production of high optical quality PWO crystals needed for the project CERN ALICE (Switzerland) [13–16]. Several physical properties of the PWO crystal are summarized in Table 1. The fabrication of the lead tungstate charge was performed with the use of ceramic technology utilizing high temperature solid phase synthesis [13] of pure oxides of lead (Pb_3O_4) and tungsten (WO_3) from their homogeneous mixture [17]. The dopant in the form of the Holmium oxide (Ho_2O_3) of various concentrations was added to the melt before the crystal growth. Five experimental Ho:PWO crystals were grown with Ho concentrations of 0.2, 0.5, 1, 2, and 4 at.%. From each crystal two rectangular shaped ($5 \times 5 \times 10$ mm) samples were cut along (0 0 1) and (1 0 0) orientations and polished with parallelism of opposite faces better than 20 arcsec and flatness of $\lambda/10$. In addition another undoped PWO crystal was grown. A $10 \times 10 \times 30$ mm sample was cut along the (1 0 0) axis from this undoped crystal. Furthermore, from the crystals of concentration 0.5% and 1.0% 5×40 mm cylindrical rods were made oriented along the (1 0 0) axis. The cutting, grinding, and polishing of the Ho:PWO elements was performed with the equipment [18] used for the mass production of PWO scintillators for the CERN ALICE project. It is assumed that Ho dopant presumably substitutes Pb ions in the PWO crystal. In this case, 1 at.% of Ho concentration corresponds to 1.1×10^{20} of Ho ions per cm^3.

Table 1
Physical properties of the $PbWO_4$ crystal [3,5,12]

Classification	Negative uniaxial
Symmetry	Tetragonal
Space group	C_{4h}^6
Unit cell	$a = 5.456$; $c = 12.020$
Refractive index at 700 nm	$n_0 = 2.221 \pm 0.009$; $n_e = 2.156 \pm 0.009$
Hardness, Mohs scale	4–5
Melting point	1123 C
Density	8.23 g/cm^3
Strongest active Raman mode at $\Delta\nu_R$	901 cm^{-1}
Raman mode linewidth at RT	4.7–4.3 cm^{-1}

3. Experimental

Room temperature (RT) absorption measurements in the visible and mid-IR spectral regions were performed with Shimadzu "UV–VIS–NIR-3101PC" and Bruker "Tensor-27" FTIR spectrophotometers. Unpolarized absorption spectra were measured at low temperatures with a close-cycle helium cryostat (Janis Research Co, Inc., Model CCS-450) and a computer-controlled 0.75 m Acton Research "SpectraPro-750" spectrometer. The kinetics of fluorescence and fluorescence spectra were measured using the Acton Research ARC-300i spectrometer with InSb detector. As an excitation source we used the 1908 nm radiation of CW Tm-fiber laser (Model TLR-30-1908, IPG Photonics Corporation). Experiments on Raman scattering in the mid-IR spectral range were made using "EKSPLA" optical parametrical generator (OPG) PG 401. OPG provides radiation tunable over 420–2300 nm spectral range with pulse duration 20–30 ps, spectral width <6 cm^{-1}, and repetition rate of 10 Hz.

4. Spectroscopic results and discussion

Fig. 1A shows RT absorption spectrum of Ho (4%):PWO crystal in the UV–visible spectral range. One can see that the fundamental UV absorption edge overlaps with holmium 361 nm transition from the ground state $^5I_8$ to $^3H_6$ multiplet.

One of the main uses for PWO in this work was the examination of its utilization as a gain material for the mid-IR spectral range. For finding the fundamental mid-IR absorption edge, we compare the FTIR spectra of doped and undoped crystals. The RT absorption spectra of PWO undoped and Ho (4%) doped crystals over the 2–10 μm range are shown in Fig. 1B. As one can see from the graph, the PWO absorption spectrum begins from ~4 μm and consists of several bands. In the measured spectra, besides the small difference in the absorption after 7 μm, the difference between the doped and the undoped crystals is negligible. It is interesting that even though the absorption of the crystal started from 3.9 μm, the crystal has a window of transparency, with a small loss, in the important IR spectral range of 4.5–4.9 μm. For the PWO crystal, featuring effective optical phonon of $\nu = 901$ cm^{-1}, the attainment of stimulated Raman over 4.5–4.9 μm range requires pumping wavelengths to be in the range of 3.2–3.4 μm. This range of pumping wavelengths falls within the range of high PWO crystal transparency. Because of this, regardless of the existing absorption band

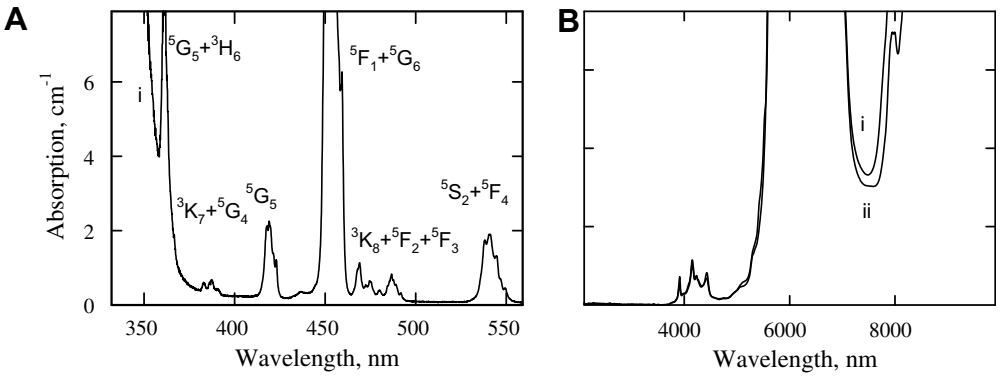

Fig. 1. UV–visible (A) and mid-IR (B) absorption spectra of Ho(4%):PWO (i) and undoped PWO crystals (ii).

of PWO around 4.1 μm, it is very possible to obtain the stimulated Raman with wavelengths up to 4.9 μm. The strongest absorption bands of the Ho^{3+}(4%):PWO crystal in the red-near-IR spectral range are shown in the Fig. 2.

The most attractive transition for laser application is the one at 2 μm from the ground state $^5I_8$ to the nearest $^5I_7$ multiplet and is depicted in Fig. 3 curve (ii). For comparison, Ho^{3+} absorption in the YAG crystal is also shown in Fig. 3 curve (iii). As one can see from Fig. 3 the Ho^{3+} ions in the PWO crystal feature smaller multiplet splitting than for the Ho^{3+}:YAG: in the YAG crystal the $^5I_8 \rightarrow {}^5I_7$ excitation corresponds to the absorption range of 1.83–2.13 μm ($\Delta\nu \approx 762$ cm^{-1}), while in the PWO crystal it corresponds to the range of 1.9–2.08 μm ($\Delta\nu \approx 460$ cm^{-1}). Other significant dissimilarities relate to the differences in the absorption spectra profiles: while in the YAG crystal the absorption band is formed by the superposition of the set of the narrow absorption lines with the bandwidth of only several nanometers, the absorption in the PWO crystal is due to the superposition of several strongly broadened lines (e.g. the 1956 nm line has FWHM of 28 nm). The shapes of the absorption bands were the same in all the Ho:PWO crystals in the studied 0.2–4 at.% range of their concentration; hence, no inhomogeneous broadening associated with different Ho concentrations was observed. In contrast to Ho:YAG's absorption, one of the possible reasons for larger Ho:PWO absorption band broadening at RT can be a stronger overlap of the Stokes components in the PWO crystal due to a smaller energy level splitting. Another reason can be due to a different crystal field variation near holmium site—trivalent Ho ions occupying Pb^{2+} sites in Ho:PWO can experience charge compensation altered with respect to Ho:YAG's, giving rise to a larger crystal field non-uniformity. The PWO crystals are uniaxial and two polarized spectra are necessary to characterize the electrical dipole transitions. However, as it was pointed out in [19], the considered transitions in holmium are magnetic-dipole allowed and, therefore, three types of polarized spectra are necessary to characterize the optical properties: (a) $E \perp z$, $H \perp z$, $k \parallel z$; (b) $E \perp z$, $H \parallel z$, $k \perp z$; (c) $E \parallel z$, $H \parallel z$, $k \perp z$. The results of the polarized measurements of the $^5I_8 \rightarrow {}^5I_7$ Ho^{3+} absorption at RT are depicted in Fig. 4. As one can see the largest coefficient of absorption corresponds to the excitation light propagating along the PWO crystal optical axis (curve iii). The difference in the absorption in the cases (iii) and (ii) can be explained by the input of magnetic-dipole transitions. In the case of incident radiation with $E \parallel z$ polarization (i), the peak absorption of Ho is only 10% smaller than in the cases of (iii) and (ii); however, for this polarization their absorption peaks for both short wave and long wave regions of the spectra are more pronounced. Because of this, this polarization looks attractive from the point of view of the realization of Ho lasing under

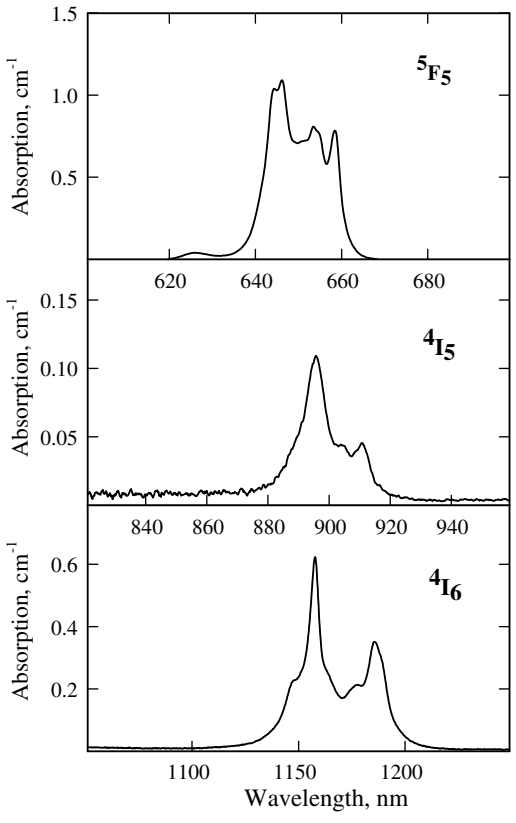

Fig. 2. Absorption spectra of the Ho(4%):PWO in the red and near-IR spectral regions.

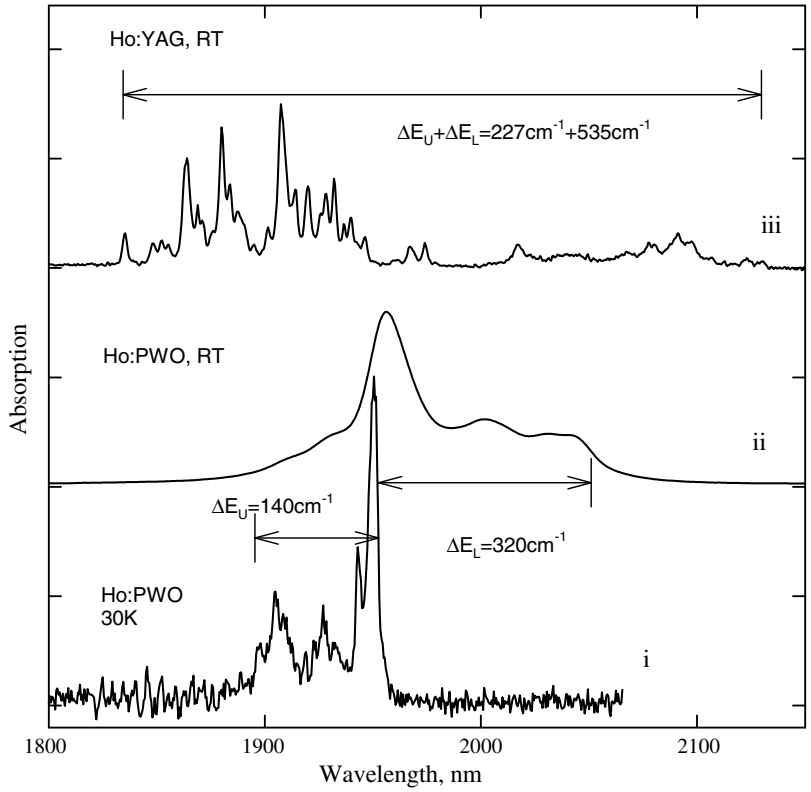

Fig. 3. Absorption spectra of Ho^{3+} ions at $^5I_8 \rightarrow {}^5I_7$ transition in PWO crystal at $T = 30$ K (i) and room temperature (ii). Room temperature absorption spectra of: Ho:YAG crystal (iii) is shown for comparison.

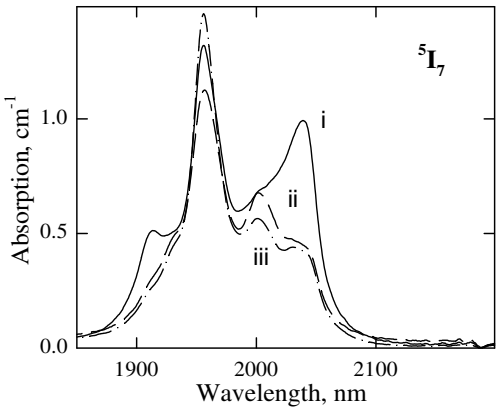

Fig. 4. Polarized $^5I_8 \rightarrow {}^5I_7$ absorption spectra of Ho(4%):PWO crystal at room temperature for $E \parallel z$ (i), $H \parallel z$ (ii); $k \parallel z$ (iii) polarizations of incident light.

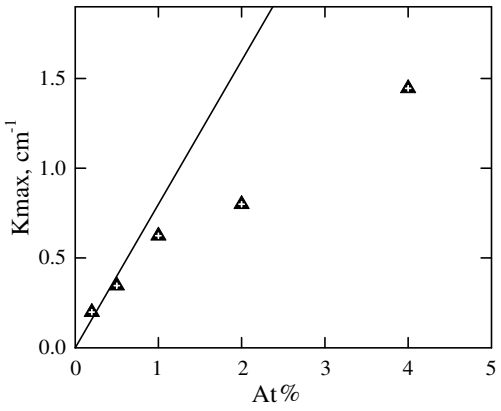

Fig. 5. Dependence of the maximum absorption coefficient at 1956 nm versus Holmium concentration.

resonance excitation of the $^5I_8 \rightarrow {}^5I_7$ transition. The dependence of the peak absorption coefficient as a function of the Ho concentration is demonstrated in Fig. 5. As it can be seen from the figure, for low concentration of Ho ions the dependence is linear, while for the high concentrations the peak absorption starts to roll-off from the linear dependence. Technological factors could be the most probable reasons for this behavior; in particular, it could be due to the saturation of Ho doping of the PWO crystal with the increase of Ho concentration in the melt.

The lifetime of $^5I_7$ state in the Ho(0.5%):PWO crystal was measured to be $\tau = 6.1$ ms at RT and $\tau = 5.0$ ms at 77 K (see Fig. 6A, curves i and ii, respectively). We believe that this difference can be explained by fluorescence trapping (see for example [20] and references herein). Strong luminescence trapping can be explained by the strong overlap of the absorption and luminescence bands due to relatively small level splitting, as well as the high quantum yield of luminescence. The weakening of luminescence trapping at low temperatures can be due to a smaller overlap of absorption and emission spectra. The most pronounced

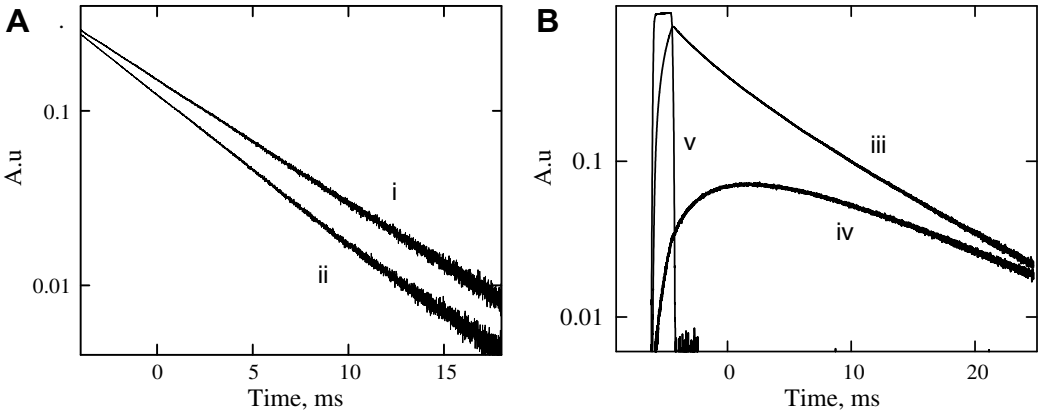

Fig. 6. (A) Kinetics of Ho^{3+} luminescence at $^5I_7 \rightarrow {}^5I_8$ transition for Ho(0.5%):PWO at RT (curve i) and $T = 77$ K (curve ii). (B) Kinetics of Ho(4%):PWO crystal at RT. Curves demonstrate kinetics of luminescence measured from the pumped region (iii) and collected from the unexcited part of the sample at ~4 mm from the excited zone (iv). Curve (v) demonstrates temporal profile of the pump radiation.

effect of luminescence trapping was observed with the highly concentrated Ho(4%):PWO sample. The Ho(4%):PWO crystal with 5 mm thickness features luminescence decay with the lifetime of $\tau \approx 14$ ms; i.e. approximately a three-fold increase with respect to the lifetime of the excited state measured for the low concentrated sample. This luminescence lifetime was practically independent of pump intensity over a wide range (0.6–10 W) of incident pump power. At the same time, the decrease of the sample thickness to 1 mm led to the luminescence lifetime shortening ($\tau \approx 7.3$ ms) practically to the value of the lifetime observed for the weakly doped crystal. To demonstrate that the observed luminescence lifetime increase is actually related to the fluorescence trapping effect we compared luminescence signals collected from the excited (Fig. 6B, curve iii) and unexcited regions of the sample when the signal from the pumped region was blocked by the diaphragm (Fig. 6B, curve iv). The spatial separation between the pumped region and the region from which the luminescence signal was collected was approximately equal to 4 mm. As it can be seen from the Fig. 6B, curve (iv), the signal is essentially non-exponential, and it is interesting to note that the signal of luminescence reached a maximum value after 2 ms delay compared to the pumping pulse.

The cross-section of absorption of Ho ions was calculated with the use of the linear extrapolation of the coefficient of absorption for low concentrations of Ho (see Fig. 4). Emission cross sections at RT are determined using either the reciprocity method (RM) or the Fuchtbauer–Landenburg equation. According to RM method the absorption and emission cross sections are related as:

$$\sigma_{em}(\nu) = \sigma_{ab}(\nu)\frac{Z_l}{Z_u}\exp([E_{zl} - h\nu]/kT), \quad (1)$$

where E_{zl} is the energy separation between the lowest crystal field components of the upper and lower states, Z_u, Z_l are partition functions that can be obtained using the energy gap (E_i, E_j) from the lowest crystal field level of each manifold, and (g_i, g_j) energy-level degeneracies obtained using the following equations:

$$Z_u = \sum_j g_j \exp(-\Delta E_j/kT), \quad (2)$$

$$Z_l = \sum_i g_i \exp(-\Delta E_i/kT). \quad (3)$$

The Z_l/Z_u factor depends on temperature but does not have any spectral dependence. For finding the Z_l/Z_u factor and E_{zl}, the absorption spectrum of Ho (4%):PWO at $T = 30$ K was measured (see Fig. 3 curve i), in addition to the RT measurements. As seen from the figure, the zero line transition corresponds to 1951 nm and practically coincides with the maximum of absorption at room temperature. It was not the goal of this work to determine the complete Stark level structure; however, the measured absorption spectrum makes it possible to estimate the energy splitting of the $^5I_7$ multiplet $\Delta E_u \approx 140\ cm^{-1}$. The comparison of the absorption spectra measured at $T = 30$ K and RT allows us to also estimate the energy splitting of the ground state $\Delta E_L \approx 320\ cm^{-1}$. These measurements along with the known stark structures of holmium in other crystals allow sufficiently accurate evaluations of the Z_l/Z_u value in the PWO crystal without knowing the precise levels position. At first, we will comment that in crystals, with a small level splitting (ΔE_l, $\Delta E_u << kT \approx 207\ cm^{-1}$), the Z_l/Z_u factor is equal to the ratio of level degeneracies, i.e. $Z_l/Z_u = g_u/g_l \approx 1.13$. One crystal of the tungstate group with a well established level structure of Holmium appears to be Ho:$CaWO_4$ [21]. The level splitting and the partition function in this crystal are calculated according to data from [21]: $\Delta E_l = 325\ cm^{-1}$, $\Delta E_u = 140\ cm^{-1}$, and $Z_l/Z_u = 0.81$. As seen, the parameters of the multiplet splitting in these crystals are very similar to each other (in crystal PWO the splitting is negligibly smaller); therefore, for the calculation of the cross-section of luminescence we used the value of $Z_l/Z_u = 0.85$. The polarized emission spectra calculated according to the Eqs. (1)–(3) are demonstrated in the Fig. 7 curve (ii).

On the other hand the emission spectra in cross-section units can be obtained with the use of the Fuchtbauer–Landenburg equation:

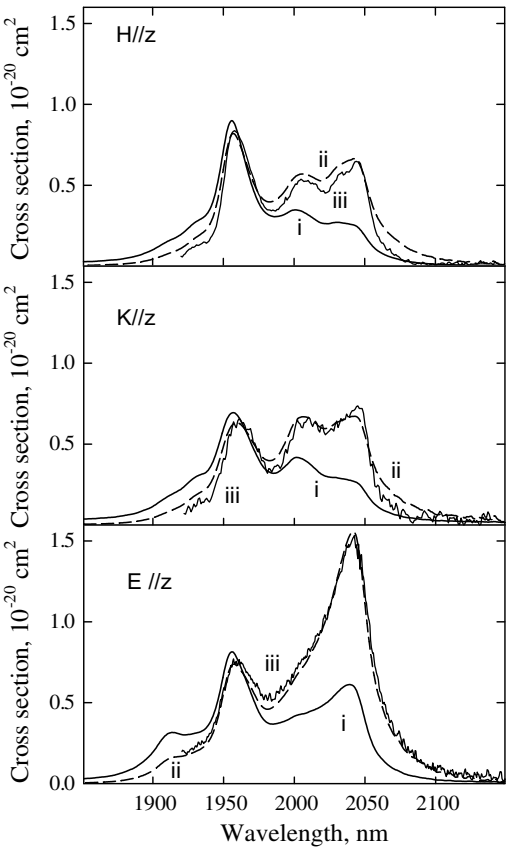

Fig. 7. RT Absorption (i, solid line) and emission spectra calculated using reciprocity method (ii dash line) and Fuchtbauer–Landenburg equation (iii) for different light polarizations.

$$\sigma_{em}(\lambda) = \frac{\lambda^5 I(\lambda)}{8\pi c n^2 \tau_{rad} \int I(\lambda)\lambda d\lambda}, \quad (4)$$

where λ – emission wavelength, $n = 2.2$ – refractive index, c – speed of light, τ_{rad} – radiative emission lifetime, and I – intensity of luminescence. In our calculations we assumed that the radiative lifetime is close to $\tau = 5$ ms (Ho lifetime measured at 77 K in a weakly (0.5%) concentrated sample). Polarized RT emission spectrum $I(\lambda)$ were measured using Acton Research ARC-300i spectrometer under 1908 nm Er-fiber laser excitation. As one can see from Fig. 7, both methods (FL and RT) demonstrate very similar calculated emission cross section profiles. Maximum value of Ho:PWO absorption cross-section is $\sigma_{ab} \approx 1.6 \times 10^{-20}$ cm^2 at 1956 nm and $H \parallel z$ polarization of incident light. On the other hand, the maximum value of the emission cross-section is $\sigma_{em} \approx 0.9 \times 10^{-20}$ cm^2 at 2045 nm for $E \parallel z$ polarization.

5. Raman scattering experiments

Fiber-bulk hybrid lasers utilizing Er^{3+}, Tm^{3+}, and Ho^{3+} doped gain media operating at 1.6, 1.9, and 2.1 μm, respectively are widely used at present. Recently SRS measurements in $BaWO_4$ crystals under 1.9 μm and 1.6 μm pumping were reported in [22]. One of the aims of the present work was to perform similar SRS studies in PWO crystals under 1.6 and 2.0 μm excitation. To study the stimulated Raman scattering in the PWO crystal in the mid-IR spectral range, we used the optical set-up shown in Fig. 8. PG-401 EKSPLA OPG was used as a pump source and provided tunable radiation with pulse duration of ~25 ps and better than 12% pulse to pulse output energy stability. Pump radiation was focused into the nonlinear PWO Raman crystal by a lens with the focal length of 250 mm. The PWO Raman crystal was 29 mm long with plane-parallel optical faces without antireflection coating. The PWO crystal was placed in the focus of the pumping beam. The pulse energy measurements for SRS and pump pulses were provided by an EMG power meter from "Molectron". Spatial energy distributions were determined by the standard knife-edge method (scanning the knife's edge in the direction perpendicular to the direction of the beam propagation and corresponding measure of transmitted energy). The experimental results of 1.7 μm radiation fits Gaussian spatial distribution with $w = 0.194$ μm FWHM. All stimulated Raman experiments were made at RT.

One of the goals of this work was the investigation of the PWO SRS threshold for 2.5 μm first and second Stokes generation. It is well known that the SRS threshold nonlinearly increases with the increase of the pump wavelength. On the other hand, the threshold for SRS of the second Stokes at 2.5 μm can be significantly lower than the threshold for the first Stokes at the same wavelength [22]. This phenomenon is important from the practical point of view since SRS thresholds in the mid-IR can be close to the level of optical damage of the used nonlinear crystals. In the current work we used pumping radiation with wavelengths 2017 and 1702 nm. PWO crystals feature an effective Raman scattering with a frequency shift of 901 cm^{-1}. In result, the second SRS Stokes in PWO under 1702 nm pumping practically coincides with the first Stokes under 2017 nm excitation (2455 and 2565 nm, respectively).

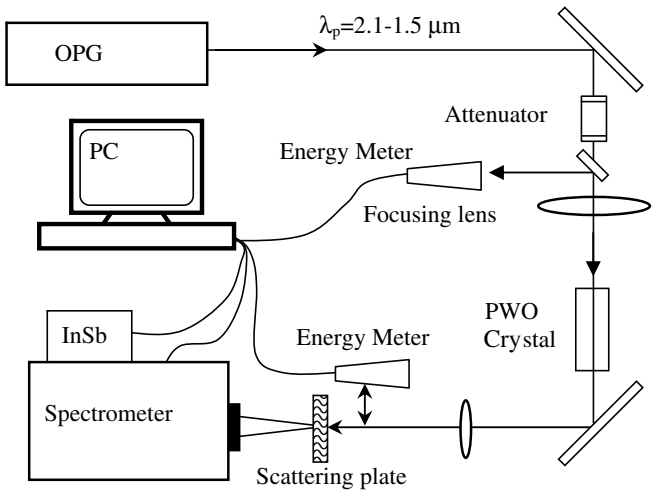

Fig. 8. Experimental setup for stimulated Raman measurements.

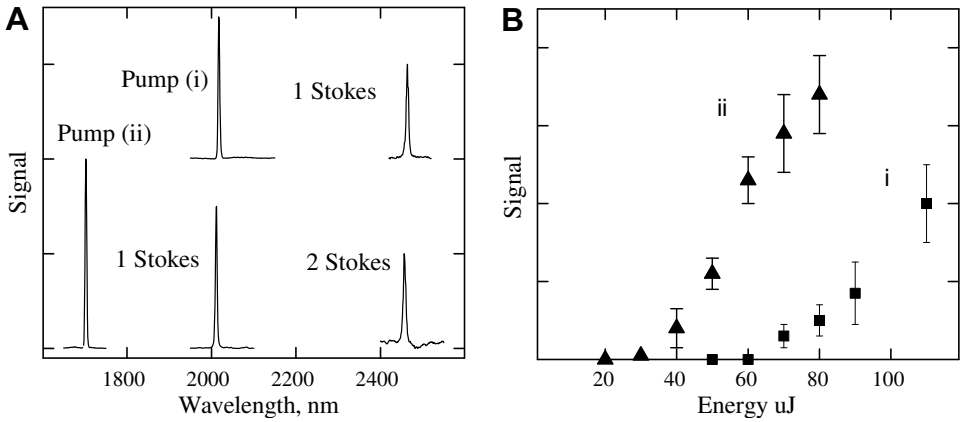

Fig. 9. Spectra (A) and stimulated Raman scattering output signals (B) at 2.5 μm for different pumping wavelength: (i) 1st Stokes under 2017 nm pumping; (ii) 2nd Stokes under 1702 nm pumping.

The measured spectra of the SRS radiations under 1702 and 2017 nm pumping are depicted in Fig. 9A. Fig. 9B demonstrates plots of the relative energy of SRS pulses at 2.5 μm as a function of the pump pulse energy. To measure input–output dependences, 1024 pulse Raman signals were accumulated at each pump energy. Maximum efficiency of SRS conversion of pump to 2.5 μm radiation was of the order of several percent. As one can see the threshold for the 2.5 μm first Stokes generation under 2017 nm excitation is ~60 μJ. On the other hand, the threshold for the second Stokes generation at the same wavelength was approximately twice smaller. Our experiments also showed that the SRS threshold for the second Stokes generated by 1702 nm pulses practically coincided with the threshold level of the first Stokes. The physical reason for such behavior was suggested in Ref. [22] and can be explained by two factors. First of all, SRS threshold significantly increases with pumping wavelength shifting to mid-IR spectral region. Second, in the case of second Stokes generation at 2.5 μm, the pump (1.7 μm) and first Stokes (2.0 μm) radiations contribute to the seeding for second stokes generation (2.5 μm) due to four-wave parametric process. This seeding is absent in the case of first stokes generation (2.5 μm) under 2.0 μm radiation pumping. Hence, it was shown that for PWO crystal a multi-stage SRS conversion of the pump radiation to the 2.5 μm spectral range is more efficient than single-cascade conversion.

6. Conclusions

In conclusion, the absorption and luminescence properties of Ho:PWO crystals in the visible and middle infrared spectral ranges were studied at room and low temperatures. The inhomogeneous broadening associated with different Ho concentrations was not observed and the shape of the absorption band was the same in the 0.2–4 at.% range of holmium concentration. The maximum absorption cross section was estimated to be $\sigma_{ab} \approx 1.6 \times 10^{-20}\,cm^2$ at 1956 nm and $H \| z$ polarization of incident light. The measured luminescence life-time at $^5I_8 \rightarrow {}^5I_7$ transition was equal to 5 ms. The maximum value of emission cross-section was calculated to be $\sigma_{em} \approx 0.9 \times 10^{-20}\,cm^2$ at 2045 nm for $E \| z$ polarization.

Stimulated Raman scattering in PWO crystals was investigated under 2.0 and 1.7 μm excitations. Our SRS experiments demonstrated that the threshold for the 2.5 μm first Stokes generation under 2017 nm excitation was approximately twice bigger than the threshold for the second Stokes generation at the same wavelength under 1702 nm wavelength excitation. The results show that Rare-Earth doped PWO crystals can be promising as a self-SRS laser media operating in the mid-IR spectral region.

Acknowledgements

The authors would like to thank Professor Tasoltan Basiev for helpful discussions and IPG Photonics Corporation for providing the Tm-fiber laser. This material is based upon work supported by the National Science Foundation under Grant Nos. EPS-0447675 and BES-0521036.

References

[1] F.A. Kröger, Some Aspects of the Luminescence of Solids, Elsevier, Amsterdam, 1948.
[2] Compact Muon Solenoid Technical Proposal, CERN/LHCC 94-38, LHCClPl, 1994.
[3] A.A. Kaminskii, H.J. Eichler, K. Ueda, N.V. Klassen, B.S. Redkin, L.E. Li, J. Findeisen, D. Jaque, J. Garcia-Sole, J. Fernandez, R. Balda, Appl. Opt. 38 (1999) 4533.
[4] A.A. Kaminskii, C.L. Mccray, H.R. Lee, S.W. Lee, D.A. Temple, T.H. Chyba, W.D. Marsh, J.C. Barnes, A.N. Annankov, V.D. Legun, H.J. Eichler, G.M.A. Gad, K. Ueda, Opt. Commun. 183 (2000) 277.
[5] T.T. Basiev, A.A. Sobol, Yu.K. Voronko, P.G. Zverev, Opt. Mater. 15 (2000) 205.
[6] W. Chen, Y. Inagawa, T. Omatsu, M. Tateda, N. Takeuchi, Y. Usuki, Opt. Commun. 194 (2001) 401.
[7] C.D. Nabors, J. Ochoa, T.Y. Fan, A. Sanchez, H.K. Choi, G.W. Turner, IEEE J. Quantum Electron. 31 (1995) 1603.
[8] P.A. Budni, M.L. Lemons, J.R. Mosto, E.P. Chiklis, IEEE J. Sel. Top. Quantum Electron. 6 (2000) 629.

[9] D.Y. Shen, W.A. Clarkson, L.J. Cooper, R.B. Williams, Opt. Lett. 29 (2004) 2396.
[10] A. Dergachev, P.F. Moulton, T.E. Drake, Proc. OSA (ASSP) 89 (2005) 608.
[11] E. Lippert, G. Rustad, S. Nicolas, G. Arisholm, K. Stenersen, Proc. SPIE 5620 (2004) 56.
[12] S. Baccaro, L.M. Barone, B. Borgia, F. Castelli, F. Cavallari, I. Dafinei, F. de Notaristefani, M. Diemoz, A. Festinesi, E. Leonardi, E. Longo, M. Montecchi, G. Organtini, Nucl. Instrum. Methods A 385 (1997) 209.
[13] S.F. Burachas, S.Ya. Beloglovski, D.V. Elizarov, I.V. Makov, V.A. Masloboev, R.M. Nikitin, Yu.A. Saveliev, A.A. Vasil'ev, M.S. Ippolitov, V.I. Man'ko, S.A. Nikulin, A.L. Apanasenko, Surface 2 (2002) 5.
[14] S. Burachas, S. Beloglovski, I. Makov, Y. Saveliev, N. Vassilieva, M. Ippolitov, V. Manko, S. Nikulin, A. Vassiliev, A. Apanasenko, G. Tamulaitis, J. Cryst. Growth 242 (2002) 367.
[15] S. Burachas, S. Beloglovsky, D. Elizarov, I. Makov, Yu. Saveliev, N. Vassilieva, M. Ippolitov, V. Manko, S. Nikulin, A. Nyanin, et al., Nucl. Instrum. Methods A 537 (2005) 185.
[16] S. Burachas, S. Beloglovski, N. Vassilieva, et al., Crystallogr. Rep. 50 (2005) S111.
[17] A.E. Dossovitski, A.L. Mikhlin, A.N. Annenkov, Nucl. Instrum. Methods A 486 (2002) 98.
[18] S. Beloglovski, S. Burachas, N. Vassilieva, et al., Crystallogr. Rep. 50 (2005) S116.
[19] S.A. Payne, L.L. Chase, L.K. Smith, W.L. Kway, W. Krupke, IEEE J. Quantum Electron. 28 (1992) 2619.
[20] S. Guy, Phys. Rev. B 73 (2006) 144101.
[21] D.E. Wortman, D. Sanders, J. Chem. Phys. 53 (1970) 1247.
[22] T.T. Basiev, M.N. Basieva, M.E. Doroshenko, V.V. Fedorov, V.V. Osiko, S.B. Mirov, Laser Phys. Lett. 3 (2006) 17.